Impact of implementing the Meyer-Neldel behavior of carrier emission pre-factors in solar cell and optical detector modeling

Francisco A. Rubinelli and Helena Ramirez

Citation: Journal of Applied Physics **117**, 104513 (2015); doi: 10.1063/1.4914038
View online: http://dx.doi.org/10.1063/1.4914038
View Table of Contents: http://scitation.aip.org/content/aip/journal/jap/117/10?ver=pdfcov
Published by the AIP Publishing

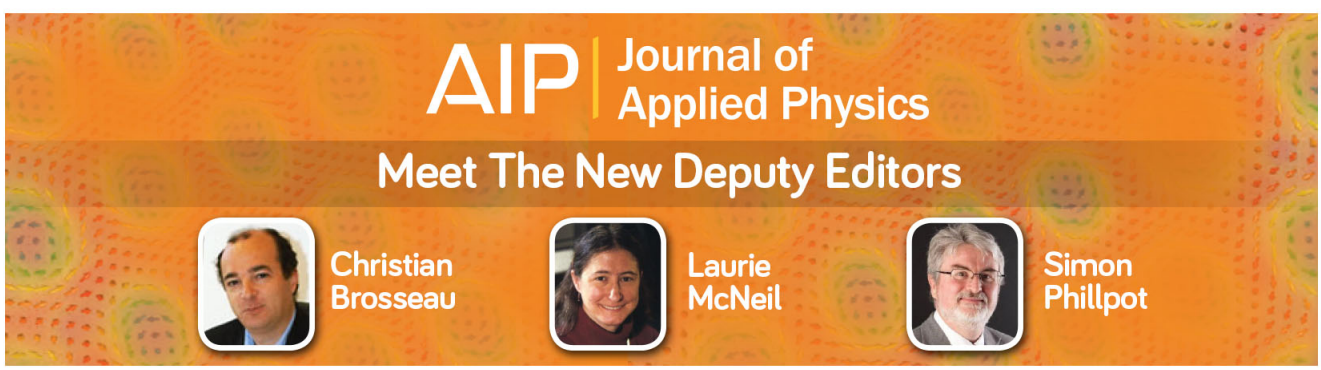

Impact of implementing the Meyer-Neldel behavior of carrier emission pre-factors in solar cell and optical detector modeling

Francisco A. Rubinelli[a] and Helena Ramirez[a]
INTEC, Conicet, Universidad Nacional del Litoral, Güemes 3450, 3000 Santa Fe, Argentina

(Received 3 February 2014; accepted 21 February 2015; published online 13 March 2015)

The Meyer-Neldel behavior reported for the emission probabilities of electrons and holes was included in our code, replacing the gap state capture cross sections of the Shockley-Read-Hall formalisms with capture cross sections containing an exponential function of the trap energy depth. The Meyer-Neldel energies for electrons and holes are the slopes of these exponentials. Our results indicate that emission probabilities of neutral states no deeper than approximately 0.45 eV and 0.37 eV from the conduction and valence band edges, respectively, can show a Meyer-Neldel behavior only, while on the other hand, its implementation in deeper gap states makes the replication of experimental J-V curves of p-i-n solar cells and detectors impossible. The Meyer-Neldel behavior can be included in all neutral capture cross sections of acceptor-like tail states without affecting the J-V characteristics, while it cannot be included in all capture cross sections of neutral donor-like tail states and/or defect states without predicting device performances below the experimental figures, that become even lower when it is also included in charged capture cross sections. The implementation of the anti Meyer-Neldel behavior at tail states gives rise to slightly better and reasonable device performances. © *2015 AIP Publishing LLC*.
[http://dx.doi.org/10.1063/1.4914038]

I. INTRODUCTION

The a-Si:H density of gap states (DOS) contains two types of localized states: tail and defect states. The distributions of tail states are decreasing exponentials, one with acceptor-like states connected to the conduction band, and one with donor-like states, connected to the valence band. Defect states, originated by dangling bonds (DB), show an amphoteric character, i.e., they can occupy three charge states: positively charged when unoccupied, neutral when singly occupied, and negatively charged when doubly occupied. A defect state can be described by two correlated energy levels: one level $E^{+/0}$ related to the +/0 transition and another level $E^{0/-}$ related to the 0/− transition. The energy difference between these levels is called the correlation energy U, the energy needed to add a second electron to a single occupied DB. The structural disorder is represented by Gaussian distributions. Defect states can also be modeled with the decoupled approximation like a pair of uncorrelated single-electron states: a donor-like level positioned at $E^{+/0}-kTln(2)$ and an acceptor-like level positioned at $E^{0/-}+kTln(2)$ (Refs. 1 and 2) because in a-Si:H the correlation energy U is much larger than the thermal energy and capture cross sections of charged states are higher than capture cross sections of neutral states.[3] Defect states are normally represented in a-Si:H based devices by three Gaussian distributions of amphoteric states recognized as D^-, D^0, and D^+, which in this paper are approximated by three pairs of Gaussians with donor-like and acceptor-like states separated in energy by $U+2kTln(2)$.[3]

The rich structure of traps present in the mobility gap makes the performance of a-Si:H based electronic devices highly dependent on the DOS. The electric field, that separates the photo-generated free carriers in the intrinsic layers of single and multiple p-i-n junctions, could be weakened by carrier trapping at gap states that, in turn, would give rise to an increase of the recombination rate and to a reduction of the collected carriers at external contacts. These effects might have a serious impact on the final efficiency of solar cells and detectors. Hence a careful evaluation of the trapped charge concentrations, recombination rates, and the electric field is essential.

In the decoupled state approximation, the occupation function, the charge density, and the net recombination rate at each energy level are defined by four competing processes in the theory of Shockley-Read-Hall (SRH). The pre-factors of the emission rates are assumed to be identical for the same species of traps regardless of their energies.[4] The condition of identical emission rate pre-factors is equivalent to the condition of identical capture cross sections. However, it has been claimed that temperature-dependent emission coefficients on traps show large variations of the emission pre-factors for varying traps.[5] A Meyer-Neldel behavior (MNB) for the emission pre-factor was reported by Antoniadis and Schiff[6] and others researchers.[7–10] These findings were used in the interpretation of drift mobilities measured with Time of Flight (TOF).[10] Device structures used in the TOF experiments are similar to the ones used in solar cells and optical detectors.

To our knowledge, the consequences of taking into account the MNB in the carrier emission pre-factors have not been explored yet in device modeling. The inclusion of the MNB in the electronic transport kinetics is expected to affect trapped carrier concentrations and the recombination rate, and therefore the predicted current-voltage and spectral response characteristic curves of solar cells and optical detectors. In this paper, the impact of including the MNB in

[a]Tel.: +54-342-4559175. Fax: +54-342-4550944.

the emission coefficients of free carriers on the current-voltage characteristics of solar cells and optical detectors is explored.

II. MOTIVATIONS

The physics used to describe the electrical transport in thin film device modeling and material characterization techniques should be consistent. Extended state mobilities can be extracted from drift mobilities measured with TOF. Light J-V characteristics and the performance of a-Si:H based devices are quite sensitive to mobilities, especially to the extended state hole mobility. The replication of the experimental Fill Factor (FF) in a-Si:H solar cells with numerical simulations becomes difficult when intrinsic layers are thick and low hole extended state mobilities and high density of defects are simultaneously adopted. This scenario can be found in a-Si:H p-i-n solar cells especially when the Defect Pool Model (DPM) is invoked to evaluate the density of defects. The DPM gives rise to a highly non-uniform density of defects that weakens the electric field intensity in the intrinsic layer bulk increasing trapping and recombination. In this scenario, extended state hole mobilities higher than usual have to be adopted in the intrinsic layer to reproduce the experimental FF.[11]

In Sec. III, the expressions of charge densities and recombination rates are conveniently modified to account for the MNB. The new equations for the occupation function, trapped charge density, and recombination rate are similar to the ones proposed by SRH but capture cross sections become dependent on the gap state energy, increasing with trap depth. Hence, the direct inclusion of the MNB in our modeling without any restrictions is expected to add more trapping and recombination that will make even more difficult the matching of experimental light J-V. In order to simplify our discussion, the analysis was undertaken by assuming a uniform density of defect states along the intrinsic layer and DBs. However, our conclusions are also valid when the concentration of DBs is evaluated with the Defect Pool model. Our input electrical parameters were calibrated by fitting experimental J-V curves of a-Si:H devices.

III. FORMALISM

In the theory developed by Shockley, Read, and Hall (SRH), four basic processes, characterized by their rates r_i, compete to define the occupation function f at the gap state:[12,13] (1) electron capture from the conduction band (r_1), (2) electron emission to the conduction band (r_2), (3) hole capture from the valence band (r_3), and (4) hole emission to the valence band (r_4). For simplicity, the rates will first be expressed without specifying the charge status of the trap. The four rates are given by

(1) Electron capture: $r_1 = n\, v_{TH}\, \sigma_n\, N_T f_p$.
(2) Electron emission: $r_2 = e_n\, N_T f_n$.
(3) Hole capture: $r_3 = p\, v_{TH}\, \sigma_n\, N_T f_n$.
(4) Hole emission: $r_4 = e_p\, N_T f_p$.

where n and p are the free carrier concentrations, v_{TH} is the thermal velocity, N_T is the trap density, f_n and $f_p = 1 - f_n$ are the occupation functions for electrons and holes, σ_n and σ_p are the electron and hole capture cross-sections, and e_n and e_p are the emission coefficients for electrons and holes, respectively. In thermal equilibrium, no net recombination occurs so $r_1 = r_2$ and $r_3 = r_4$. Using the Fermi-Dirac statistics at thermal equilibrium, the emission rates (r_2 and r_4) can be expressed as

$$e_n(E_T) = v_{TH} N_C \sigma_n \exp\left(-\frac{E_C - E_T}{kT}\right), \tag{1a}$$

$$e_p(E_T) = v_{TH} N_V \sigma_p \exp\left(-\frac{E_T - E_V}{kT}\right), \tag{1b}$$

where E_T is the trap energy, E_C is the conduction band edge, E_V is the valence band edge, and N_C and N_V are the effective conduction and valence density of states, respectively. Under non-equilibrium and at steady-state conditions, the electron and hole occupation functions f_E and f_H and the recombination efficiency η_R at E_T are expressed as[13]

$$f_E(x,E_T) = \frac{n(x) v_{TH} \sigma_n + e_p}{n(x) v_{TH} \sigma_n + p(x) v_{TH} \sigma_p + e_n + e_p}$$
$$f_H(x,E_T) = 1 - f_E(x,E_T), \tag{2a}$$

$$\eta_R(x,E_T) = {v_{TH}}^2 \sigma_n \sigma_p \frac{n(x)p(x) - n_i^2}{n(x) v_{TH} \sigma_n + p(x) v_{TH} \sigma_p + e_n + e_p}, \tag{2b}$$

where n_i is the intrinsic carrier concentration. The trapped concentrations and the recombination rate at E_T are given by the product of the trap density N_T, with the occupation function and the recombination efficiency η_R, respectively. The total trapped charge density ρ ($\mathrm{Ccm^{-3}}$) and recombination rate R ($\mathrm{cm^{-3}\ s^{-1}eV^{-1}}$) are computed by integrating the respective quantities over all the gap states.

When the donor or acceptor character of the trap is taken into account, the emission coefficients of electrons and holes (see Eq. (1)) can be re-written as

$$e_n^0(E_T) = v_{TH} N_C \sigma_n^+ \exp\left(-\frac{E_C - E_T}{kT}\right) = \omega_{+D} \exp\left(-\frac{E_C - E_T}{kT}\right), \tag{3a}$$

$$e_p^+(E_T) = v_{TH} N_V \sigma_p^0 \exp\left(-\frac{E_T - E_V}{kT}\right) = \omega_{0D} \exp\left(-\frac{E_T - E_V}{kT}\right), \tag{3b}$$

$$e_n^-(E_T) = v_{TH} N_C \sigma_n^0 \exp\left(-\frac{E_C - E_T}{kT}\right) = \omega_{0A} \exp\left(-\frac{E_C - E_T}{kT}\right), \tag{3c}$$

$$e_p^0(E_T) = v_{TH} N_V \sigma_p^- \exp\left(-\frac{E_T - E_V}{kT}\right) = \omega_{-A} \exp\left(-\frac{E_T - E_V}{kT}\right), \tag{3d}$$

where

$$\omega_{+D} = v_{TH}\sigma_n^+ N_C \quad \omega_{0D} = v_{TH}\sigma_p^0 N_V,$$
$$\omega_{0A} = v_{TH}\sigma_n^0 N_C \quad \omega_{-A} = v_{TH}\sigma_p^- N_V.$$

The first two emission processes take place from donor-like traps and the last two from acceptor-like traps. The trap energy E_T is measured positively up from E_V. As the emission probabilities are expressed in units of s^{-1}, the pre-factors can be associated to frequencies recognized as phonon or attempt-to-escape frequencies: (a) ω_{+D} for electrons emitted from donor-like states to the conduction band (e_n^0 is balanced by the capture of electrons by donor-like gap states characterized by σ_n^+); (b) ω_{0D} for holes emitted from donor-like states to the valence band (e_p^+ is balanced by the capture of holes by donor-like gap states characterized by σ_p^0); (c) ω_{0A} for electrons emitted from acceptor-like states to the conduction band (e_n^- is balanced by the capture of electrons by acceptor-like gap states characterized by σ_n^0); (d) ω_{-A} for holes emitted from acceptor-like states to the valence band (e_p^0 is balanced by the capture of holes by acceptor-like gap states characterized by σ_p^-).

The electron and hole drift mobilities μ_{nd} and μ_{pd} measured in TOF experiments can be expressed in terms of the extended state hole mobilities μ_{ne} and μ_{pe} as[14,15]

$$\mu_{nd} = \mu_{ne}\left(\frac{n}{n+n_T}\right) \approx \mu_{ne}\frac{n}{n_T}$$
$$\mu_{pd} = \mu_{pe}\left(\frac{p}{p+p_T}\right) \approx \mu_{pe}\frac{p}{p_T}, \tag{4a}$$

where n_T and p_T are the trapped electron and hole concentrations contained in gap states that can reach a state of quasi-equilibrium with extended states. The state of quasi-equilibrium is attained via trapping of carriers by gap states followed by re-emissions to higher energy conducting states while being drifted along the intrinsic layer. The transient time, t_T, is defined as the time needed for photo-generated charge carriers to cross the sample. Tiedje *et al.* defined the energies $E_{DEA\text{-}C}$ and $E_{DED\text{-}V}$ at which the release times of electrons and holes to the conduction band and valence band are equal to the electron and hole transit times t_E and t_H, respectively, as[12,16]

$$E_{DEA-C} = kT\ln(\omega_{0A}t_E) \quad E_{DED-V} = kT\ln(\omega_{0D}t_H), \tag{4b}$$

where ω_{0A} and ω_{0D} are the phonon attempt-to-escape frequencies. Electrons and holes in traps shallower than $E_{DEA\text{-}C}$ and $E_{DED\text{-}V}$, respectively, can be emitted back to the conduction band and valence band within the times t_E and t_H and collected at the external contacts. The trapped concentrations of Eq. (4a) are given by

$$n_T = \int_{E_C - E_{DEA\_C}}^{E_C} g(E_T)f_E(E_T)dE_T$$
$$p_T = \int_{E_V}^{E_V + E_{DED\_V}} g(E_T)f_H(E_T)dE_T, \tag{4c}$$

where $g(E_T)$ is the density of gap states and $f_E(E_T)$ and $f_H(E_T)$ are given by Eq. (2a). In Eqs. (4b) and (4c), only the demarcation energies that correspond to emission of carriers to the closest band were formulated. Similar expressions could be written for the emission of carriers to the opposite bands. However, transitions of carriers to the opposite bands are not likely because they would be associated to emission times far superior to the transit times t_E and t_H.

A Meyer-Neldel behavior for the emission pre-factor was proposed by Antoniadis and Schiff[6,10] that in this paper will be recognized with the symbol MNB (Meyer-Neldel Behavior). The dependence of the attempt-to-escape frequency with respect to the gap state energy E_T with the MNB is given by[10]

$$\omega_{0D} = \omega_{00D}\exp\left(\frac{E_T - E_V}{E_{MND-V}}\right), \tag{5a}$$

$$\omega_{0A} = \omega_{00A}\exp\left(\frac{E_C - E_T}{E_{MNA-C}}\right), \tag{5b}$$

where ω_{00D} and ω_{00A} are the phonon frequencies corresponding to the valence and conduction band edges for emission of holes from donor-like states to the valence band and emission of electrons from acceptor-like states to the conduction band, respectively. $E_{MND\text{-}C}$ and $E_{MND\text{-}V}$ are the Meyer-Neldel energies (MNE) associated to these transitions. Equations (3) and (5) can be combined as

$$e_p^+(E_T) = \omega_{00D}\exp\left(\frac{E_T - E_V}{E_{MND-V}}\right)\exp\left(-\frac{E_T - E_V}{kT}\right), \tag{5c}$$

$$e_p^-(E_T) = \omega_{00A}\exp\left(\frac{E_C - E_T}{E_{MNA-C}}\right)\exp\left(-\frac{E_C - E_T}{kT}\right). \tag{5d}$$

Hence, the MNB gives rise to larger emission pre-factor frequencies for deeper traps. When the concept of the MNB was invoked in TOF experiments only two of the four emission probabilities defined in Eq. (3) needed to be modified. However, there is no logical reason to exclude the MNB in the other two emission processes under steady state conditions. Using similar arguments, the attempt to escape frequencies and the emission probabilities of electrons and holes to the valence and conduction bands, respectively, could be expressed as

$$\omega_{+D} = \omega_{++D}\exp\left(\frac{E_C - E_T}{E_{MND-C}}\right) \quad \omega_{++D} = v_{TH}\sigma_n^+ N_C, \tag{6a}$$

$$\omega_{-A} = \omega_{--A}\exp\left(\frac{E_T - E_V}{E_{MNA-V}}\right) \quad \omega_{--A} = v_{TH}\sigma_p^- N_V, \tag{6b}$$

$$e_n^0(E_T) = \omega_{++D}\exp\left(\frac{E_C - E_T}{E_{MND-C}}\right)\exp\left(-\frac{E_C - E_T}{kT}\right), \tag{6c}$$

$$e_p^0(E_T) = \omega_{--A}\exp\left(\frac{E_T - E_V}{E_{MNA-V}}\right)\exp\left(-\frac{E_T - E_V}{kT}\right), \tag{6d}$$

where now ω_{++D} and ω_{--A} are the frequencies at the conduction and valence band edges for emissions of electrons

from donor-like states to the conduction band and emissions of holes from acceptor-like states to the valence band, respectively. $E_{MND\text{-}C}$ and $E_{MNA\text{-}V}$ are the Meyer-Neldel energies in correspondence with these transitions. The exponential factors of Eqs. (5) and (6) containing the Meyer-Neldel energies are always greater than unity. When very high Meyer-Neldel energies are adopted, the traditional equation (3) of the SRH formalism is recovered.

The conventional multiple-trapping model assumes that the attempt-to-escape frequencies, given by Eq. (3), are the same for all the gap states of the same trap species. Equations (5) and (6) can also be rewritten in the same form of Eq. (3) as

$$e_n^0(E_T) = v_{TH}\sigma_{n\omega}^+ N_C \exp\left(-\frac{E_C - E_T}{kT}\right), \tag{7a}$$

$$e_p^+(E_T) = v_{TH}\sigma_{p\omega}^0 N_V \exp\left(-\frac{E_T - E_V}{kT}\right), \tag{7b}$$

$$e_n^-(E_T) = v_{TH}\sigma_{n\omega}^0 N_C \exp\left(-\frac{E_C - E_T}{kT}\right), \tag{7c}$$

$$e_p^0(E_T) = v_{TH}\sigma_{p\omega}^- N_V \exp\left(-\frac{E_T - E_V}{kT}\right), \tag{7d}$$

where now the cross sections $\sigma_{n\omega}^+$, $\sigma_{p\omega}^0$, $\sigma_{n\omega}^0$, and $\sigma_{p\omega}^-$ can be expressed in terms of the conventional cross sections σ_n^+, σ_p^0, σ_n^0, and σ_p^- defined in the SRH formalism as

$$\sigma_{n\omega}^+(E_T) = \sigma_n^+ \exp\left(\frac{E_C - E_T}{E_{MND-C}}\right), \tag{8a}$$

$$\sigma_{p\omega}^0(E_T) = \sigma_p^0 \exp\left(\frac{E_T - E_V}{E_{MND-V}}\right), \tag{8b}$$

$$\sigma_{n\omega}^0(E_T) = \sigma_n^0 \exp\left(\frac{E_C - E_T}{E_{MNA-C}}\right), \tag{8c}$$

$$\sigma_{p\omega}^-(E_T) = \sigma_p^- \exp\left(\frac{E_T - E_V}{E_{MNA-V}}\right). \tag{8d}$$

Equation (8) indicates that the inclusion of the MNB in the emission probabilities of the SRH formalism can be implemented by defining energy dependent cross sections that are higher for deeper gap states. These energy dependent cross sections are identical to the conventional cross sections only at band edges. Higher cross sections are associated to more trapping and recombination. Hence, the characteristic current–voltage (J-V) of solar cells and optical detectors predicted with device computer modeling could be significantly altered when the MNB is taken into account in the emission probabilities of the SRH formalism. As the MNB was proposed for the TOF experiments, the cross sections that necessarily have to follow the exponential energy dependence are the capture cross sections for electrons at neutral acceptor-like gap states σ_n^0 and the capture cross sections for holes at neutral donor-like gap states σ_p^0 (see Eqs. 8(b) and 8(c)). Hence, the impact of the MNB in device modeling of J-V characteristics will first be explored by modifying in our code only the neutral capture cross sections.

It can be shown that when the MNB is taken into account in the carrier emission probabilities, the demarcation levels $E_{DEA\text{-}C}$ and $E_{DED\text{-}V}$ given by Eq. (4b) have to be replaced by the following expressions:[17]

$$E_{DEA-C} = \left[\frac{kTE_{MNA-C}}{(E_{MNA-C} - kT)}\right]\ln(\omega_{00A}t_E)$$
$$E_{DED-V} = \left[\frac{kTE_{MND-V}}{(E_{MND-V} - kT)}\right]\ln(\omega_{00D}t_H), \tag{9}$$

where $E_{MNA\text{-}C}$ and $E_{MND\text{-}V}$ are the MNE for transitions between acceptor-like traps and the conduction band and between donor-like traps and the valence band, respectively. The energies $E_{DEA\text{-}C}$ and $E_{DED\text{-}V}$ are higher than the ones proposed by Tiedje when $E_{MNA\text{-}C}$ and $E_{MND\text{-}V}$ are assumed positive and greater than kT.

IV. METHODOLOGY

The MNB in the emission probabilities was included in the computer code D-AMPS (Analysis of Microelectronic and Photonic Structures + new Developments)[18] by modifying the cross sections of the SRH formalism as discussed in Sec. III (Eq. (8)). D-AMPS solves the system of Poisson's equation and continuity equations for free electrons and holes with the finite differences method and the Newton-Raphson method.[6] The independent variables are the electron potential and the quasi-Fermi levels. D-AMPS is an updated version of the well-known software AMPS released by the Pennsylvania State University that includes extra features like amphoteric states, the Defect Pool-model, the Pool-Frenkel effect, a simplified treatment of light scattering, etc.[18]

The devices selected to study the impact of including the MNB in the simulated J-V curves are three layer p-i-n a-Si:H structures. Our code was appropriately calibrated by fitting measured dark and light current–voltage (J-V) characteristic curves. Samples were deposited in a multi-chamber RF-PECVD facility under identical conditions and characterized with appropriate equipment at Delft University of Technology.[19] Each device structure is as follows: TCO/p-a-SiC:H/i-a-Si:H/n-a-Si:H/Al. The front contact is an Asahi U-(SnO_2:F) type substrate with a textured surface. The p- and n-layer thicknesses are 10 nm and 20 nm, respectively. The Al back contact is 300 nm thick. The selected data correspond to a-Si:H based p-i-n junctions with intrinsic layer thicknesses of 200 nm, 40 nm, and 600 nm. Figure 1 shows our fittings of the dark J-V characteristics measured at 40 °C, and light J-V characteristics measured at room temperature under AM1.5 illumination. The resulting electrical parameters can be found in Table I. Flat band conditions were assumed at contacts to simplify our modeling and block the injection of minority carriers at doped layers. The optical parameters were obtained from measured reflection and transmission spectra on a-Si:H films. The global density of states and the Urbach slope were extracted with the Dual Beam Photoconductivity. The other electrical input parameters were conveniently adjusted to reproduce the experimental data. The Uniform Density Model (UDM), that assumes a

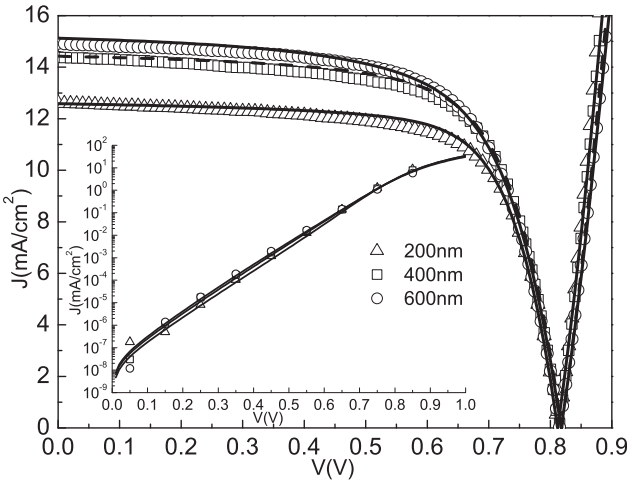

FIG. 1. Fittings of the J-V curves under AM1.5 illumination and dark conditions (inset) achieved with D-AMPS. Devices are p-i-n based a-Si:H with 200 nm (triangles), 400 nm (squares), and 600 nm (circles) thick intrinsic layers. Open symbols are the experimental data and solid lines are the fittings obtained with the parameters listed in Table I.

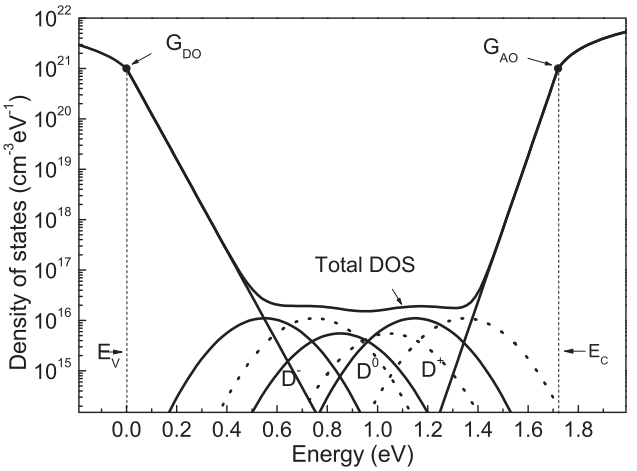

FIG. 2. Density of states in (i) a-Si:H. The donor-like and the acceptor-like distributions of tails states have an exponential dependence with the energy (straight lines) D^-, D^0, and D^+ are Gaussian distributions of donor-like (solid lines) and acceptor-like (dotted lines) defect states. The total DOS is also shown.

constant DB density in each device layer, was adopted to simplify the discussion. The correlation energy U was assumed equal to 0.2 eV.[20] In doped layers, doping densities were adjusted to reproduce the experimental activation energies.

Figure 2 shows the DOS adopted in the a-Si:H intrinsic layer: defect states described by three Gaussian distributions, recognized as D^-, D^0, and D^+ and tail states described by two decreasing exponentials with slopes E_A and E_D, respectively. The density of states G_{AO} and G_{DO} at the respective mobility band edges E_C and E_V were adopted equal to 10^{21} cm^{-3} eV^{-1}. In the optical model, the intensity, I, of the incident light was equally shared among N sub-beams with intensity I/N and with different incident angles. The model accounts for light scattering on rough surfaces by defining also angles at each interface different from 90° with respect to the incident sub-beams. These angles can vary between a maximum and a minimum value that can be selected. The total generation rate $G(x)$ of electron-hole (e-h) pairs results from adding the e-h pairs generated by each sub-beam.

V. IMPACT OF THE MEYER-NELDEL ENERGIES IN THE SOLAR CELL AND DETECTOR J-V CHARACTERISTICS

In this section, the J-V characteristics of the solar cell shown in Figure 1 are re-evaluated taking into account the

TABLE I. List of electrical input parameters resulting from our fittings. The meaning of the symbols is as follows: W is the layer thickness, E_G is the mobility gap, N_c and N_v are the effective density of states in the conduction and valence band, respectively, μ_N and μ_P are the electron and hole mobilities, E_D and E_A are the valence and the conduction tail slopes, σ_{nt} and σ_{pt} are the cross section for electrons and holes in tail states, D^-, D^0, and D^+ are the densities of states enclosed in the three Gaussians, E^-, E^0, and E^+ are the peak positions of these Gaussians, s_D are the standard deviations, σ_{ng} and σ_{pg} are the cross sections for electrons an hole in defect states. The superscripts +, 0, and − indicate the charge state of the cross sections.

Parameters	P	i-200 nm	i-400 nm	i-600 nm	n
W (nm)	10	600	600	600	20
$\mathbf{G_P}$ (eV)	1.9	1.72	1.72	1.72	1.72
Nc, Nv (cm^{-3})	3×10^{20}	3×10^{20}	3×10^{20}	3×10^{20}	3×10^{20}
$\mathbf{\mu_N}$ (cm^2 V^{-1} s^{-1})	10	20	20	20	10
$\mathbf{\mu_P}$ (cm^2 V^{-1} s^{-1})	1	3.5	3.5	3.5	1
$\mathbf{E_D}$ (meV)	80	48	48	48	50
$\mathbf{E_A}$ (meV)	30	30	30	30	30
$\mathbf{\sigma_{nt}^+\ \sigma_{pt}^-}$ (cm^2)	1×10^{-15}	2×10^{-15}	2×10^{-15}	2×10^{-15}	1×10^{-15}
$\mathbf{\sigma_{nt}^0\ \sigma_{pt}^0}$ (cm^2)	1×10^{-17}	1×10^{-16}	1×10^{-16}	1×10^{-16}	1×10^{-17}
$\mathbf{D^-}$ (cm^{-3})	3.044×10^{12}	4.8×10^{15}	4.4×10^{15}	3.6×10^{15}	6.78×10^{18}
$\mathbf{D^0}$ (cm^{-3})	2×10^{16}	2.4×10^{15}	2.2×10^{15}	1.8×10^{15}	1.6×10^{15}
$\mathbf{D^+}$ (cm^{-3})	5.254×10^{18}	4.8×10^{15}	4.4×10^{15}	3.6×10^{15}	1.51×10^{12}
$\mathbf{E_D^-}$ (eV)	0.7	0.55	0.55	0.55	0.6
$\mathbf{E_D^0}$ (eV)	1.0	0.85	0.85	0.85	0.9
$\mathbf{E_D^+}$ (eV)	1.3	1.15	1.15	1.15	1.2
$\mathbf{s_D}$ (eV)	0.13	0.13	0.13	0.13	0.13
$\mathbf{\sigma_{ng}^+\ \sigma_{pg}^-}$ (cm^2)	2×10^{-15}	9×10^{-15}	9×10^{-15}	9×10^{-15}	1×10^{-14}
$\mathbf{\sigma_{ng}^0\ \sigma_{pg}^0}$ (cm^2)	4×10^{-16}	8×10^{-16}	7.3×10^{-16}	3.5×10^{-16}	2×10^{-16}

MNB. The same electrical parameters listed in Table I, obtained from our fittings, were used to perform these new simulations. Our results will be discussed for the p-i-n junction with a 600 nm thick intrinsic layer only because they are similar for other intrinsic layer thicknesses (see Sec. VII). First, the capture cross section for electrons at neutral acceptor tail states was assumed to follow the MNB (Eq. 8(c)). The MNE proposed by Antoniadis and Schiff are around 26–28 meV.[6,10] The dark and light J-V characteristics obtained for different Meyer-Neldel energies $E_{MNA\text{-}C}$ within the range going from 26 meV to 200 meV were explored and practically identical J-V characteristics to the ones obtained without including the MNB were predicted (maximum differences $\sim$1% at V = 2 V). Hence, the enhancement in the emission probabilities generated by the MNB does not impact on the J-V characteristics, when only the capture cross section for electrons at the neutral acceptor tail states is assumed to increase at deeper states. Inspection of recombination rates and trapped electron concentration profiles indicates that there is a moderate increase of both quantities that does change the overall recombination rate and the total trapped charge concentration. However, the acceptor-like tail provides the lowest contribution to the total recombination rate among the possible four (i.e., acceptor-like tail, donor-like tail, acceptor-like Gaussians, and donor-like Gaussians). Figure 3(a) shows the changes in the recombination rate profile under short circuit conditions and AM1.5 illumination and the four contributions to the total recombination rate. The increase of the capture cross sections for electrons at neutral states given by the MNB does not significantly impact in the overall recombination rate and the trapped electron concentration due to the steepness of the conduction band tail. Modified capture cross sections become significant at energies where the density of states is already very low. Similarly, the dark and light J-V curves of optical detectors that operate at reverse voltages do not change when the MNB is included in neutral conduction band tail states.

When the capture cross section for holes at neutral donor tail states is assumed to vary with the trap energy following the MNB (Eq. 8(b)), changes in the dark J-V are not very noticeable (see Figure 4(a), where $E_{MND\text{-}V}$ was adopted 30 meV to make more visible the effect) but some modifications can be observed at high forward voltages while the modifications in the light J-V (AM1.5 illumination) can be easily be detected (see Figure 5(a)) for the Meyer-Neldel energies proposed in the literature. Our results are shown for a Meyer-Neldel energy of $E_{MND\text{-}V} = 70$ meV.[8]

At high forward voltages and under dark conditions, when the device is biased over flat band conditions and operates in the Space Charge Limited Current (SCLC) regime, the current drops slightly. The increase of the capture cross sections for holes at neutral donor traps naturally favors trapping of holes at neutral donor states. Detailed simulations indicate that free holes injected through the front contact, now find traps with much higher capture cross sections at donor tail states and become preferentially trapped at the front region of the intrinsic layer rather than in the bulk. The final result is a lower concentration of holes available to be trapped at the back region of the intrinsic layer near the i/n interface than when the MNB is not taken into account. Hence, the net trapped charge at the back region of the intrinsic layer becomes more negative. This redistribution of trapped charge inside the intrinsic layer increases the potential barrier of the virtual cathode located near the i/n interface and inside the intrinsic layer. The higher barrier of the virtual cathode lowers the injection of free electrons into the intrinsic layer and the total current flowing through the device, which is limited in the SCLC regime by injection of electrons through the virtual cathode. Changes in the current at high forward seem minor in Figure 4(a) but they are of the

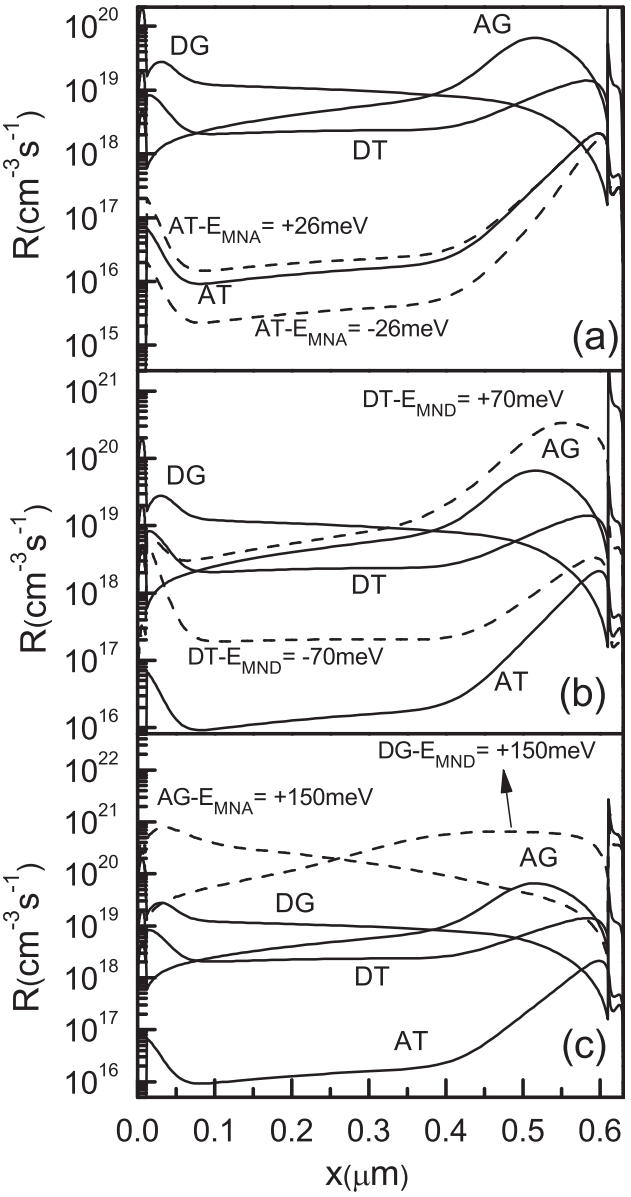

FIG. 3. Contributions to the total recombination rate coming from acceptor tail states (AT), donor tail states (DT), acceptor defect states (AG), and donor defect states (DG) without taking into account the MNB (solid lines). The same contributions are shown when the MNB is taken into account only at (a) AT, (b) DT, (c) AG, and (d) DG in dashed lines for a positive and a negative Meyer-Neldel energy of: ±26 meV at acceptor tail states, ±70 meV at donor tail states, and ±150 meV at defect states The recombination rate components are plotted at short circuit conditions and under AM1.5 illumination.

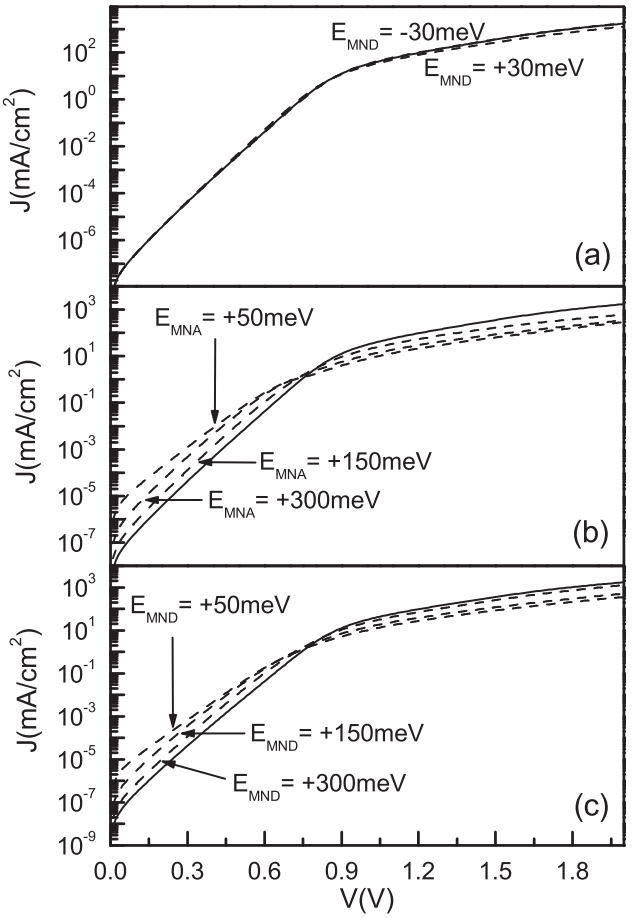

FIG. 4. Dark J-V characteristics when the MNB is taken into account at (a) donor tail states; (b) acceptor defect states; and (c) donor defect states (dashed lines) for different Meyer-Neldel energies: ±30 meV at donor tail states; 50, 100, 300 at defect states. The dark J-V characteristic when the MNB is not taken into account is shown as a solid line for comparison.

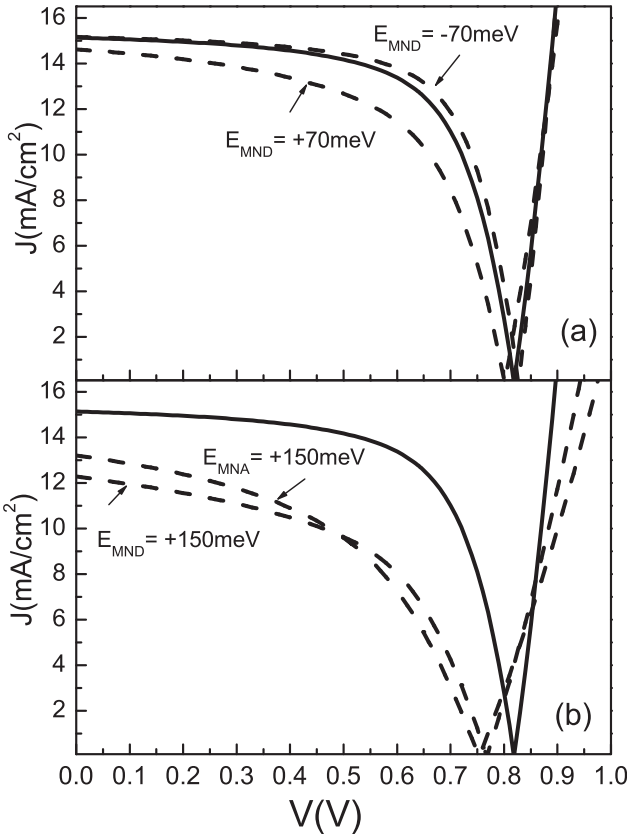

FIG. 5. Light J-V characteristics obtained when the MNB is taken into account only at the capture cross section of neutral (a) donor tail states; (b) acceptor defect states; and (c) donor defect states (dashed lines) for Meyer-Neldel energies of: (a) ±70 meV at donor tail states, (b) 150 meV at defect states. The light J-V characteristic when the MNB is not included in the emission coefficients is shown as a solid line for comparison.

order of around 28% at V = 2 V. For low forward voltages, the dark current does not show any noticeable changes when the MNB is included in capture cross sections of neutral donor-like tail states because the dark current is controlled by recombination through defect states.

Under AM1.5 illumination, a significant increase of the recombination rate and the concentration of trapped holes is observed in the middle and rear regions of the intrinsic layer rather than near the p/i interface, i.e., in regions where the concentration of free holes is lower than the concentration of free electrons. This change in the recombination rate can be observed in Figure 3(b) for a Meyer-Neldel energy of $E_{MND\text{-}V} = 70$ meV.[8] The higher recombination rate combined with a weaker electric field in the intrinsic layer due to the partial shielding introduced by the excess of trapped positive charge gives rise to p-i-n a-Si:H based solar cells with a lower FF, and in lesser extent to lower short circuit current (J_{SC}) and open circuit voltages (V_{OC}) and of course to a solar cell with poorer conversion efficiencies.

In optical detectors that operate at reverse voltages, the dark J-V curve does not show any changes when the MNB is included in capture cross sections of neutral donor-like tail states because the current is controlled by thermal generation of e-h pairs created at defect states. Under illumination, the collected current is lower due to the significant increase of the recombination rate mostly at the back region of the intrinsic layer as it was already described at short circuit conditions. There is also an increase in the concentration of trapped holes in the bulk and at the rear region of the intrinsic layer. At higher reverse voltages, the difference between the collected current narrows whether the MNB is taken into account or not.

Being more specific when the MNB is taken into account in capture cross sections of donor-like tail states, the Meyer-Neldel energy must be adopted above 200 meV and 500 meV in order to keep the relative differences below 3% in the dark and light J-V curves, respectively. These relative differences in the light J-V are given for lower voltages than at the maximum power point condition. For voltages near V_{OC}, the relative errors can become very high due to the low value of the current. For a MNE of 70 meV proposed by Cheng *et al.*,[8] the differences in the dark J-V reach nearly 30% at high forward voltages and over 20% in the light J-V.

Although for the interpretation of the drift mobilities, the concept of the MNB was explicitly used only at emission transition rates from tail states to extended states[6–10] and defect states were not usually included in the analysis except for few cases,[21] it is interesting to explore the impact of including the MNB in the emission transition rates from defect states to extended states. Our results indicate that

when the MNB is taken into account at capture cross sections of either neutral donor-like or acceptor-like defect states (Eqs. 8(b) and 8(c)) significant changes in the dark and light J-V are obtained.

An important increase of the dark current can be observed at low forward voltages (see Figures 4(b) and 4(c)) that are controlled by recombination through gap states near mid-gap. The capture cross sections that exponentially increase with the neutral trap depth give rise to a higher flow of free carriers towards the deep traps where they recombine. At low voltages, the current is limited by recombination through the traps located in the intrinsic layer bulk and closer to the p/i interface (see Figure 6(a)). When the voltage is increased more and more, traps towards the interfaces join to the recombination processes. At high forward voltages, the MNB gives rise to a significant lowering of the dark current density. There is a charge redistribution similar to the one observed when the MNB was included at neutral donor tail states. A distinction must be made between the two scenarios: when capture cross sections are assumed to be energy dependent at neutral acceptor defect states or at neutral donor defect states. In the first case, electrons that can surmount the virtual cathode become more easily trapped between the virtual cathode and the p/i interface by acceptor-like defect states that now have much higher neutral capture cross sections. In the same region, an increase of the net positive charge trapped in donor-like defect states is also observed because there are fewer electrons available to be trapped by donor-like defect states due to the bigger fraction captured by deep-acceptor states. The final result is an increase of the net negative charge (because the negative charge increases more than the positive charge) that strengthens the electric field between the p/i interface and the virtual cathode where it is positive. As the integral of the electric field along the device must remain unchanged, there should be a decrease of the electrical field somewhere else. Our simulations indicate that the magnitude of the electric field also increases between the virtual cathode and the i/n interface but in this region the field has a negative sign. Hence, the simultaneous increase of the magnitude of the electric field at both sides of the virtual cathode is accompanied by a rise of the potential barrier of the virtual cathode as can be observed in the final potential distribution shown in Figure 6(b). The higher barrier at the virtual cathode lowers the flow of electrons entering into the intrinsic layer bulk. When the MNB is implemented in donor-like defect states, the kinetics is similar but now the increase in the positive charge is caused by the higher capture cross sections present at neutral donor defect traps. Holes injected through the front contact become more easily trapped by these neutral donor defect traps with higher capture cross sections. Hence, a lower concentration of free holes will be available to become trapped by acceptor defect states. This scarcity of free holes increases the negative charge that is trapped at acceptor defect states. The final result is a net increase of the overall negative charge between the p/i interface and the virtual cathode as happened when the MNB was implemented in acceptor-like defect states. The modifications of the dark J-V when the MNB is included at capture cross sections of defect states are illustrated in Figures 4(b) and 4(c) for Meyer-Neldel energies of 50, 150, and 300 meV.

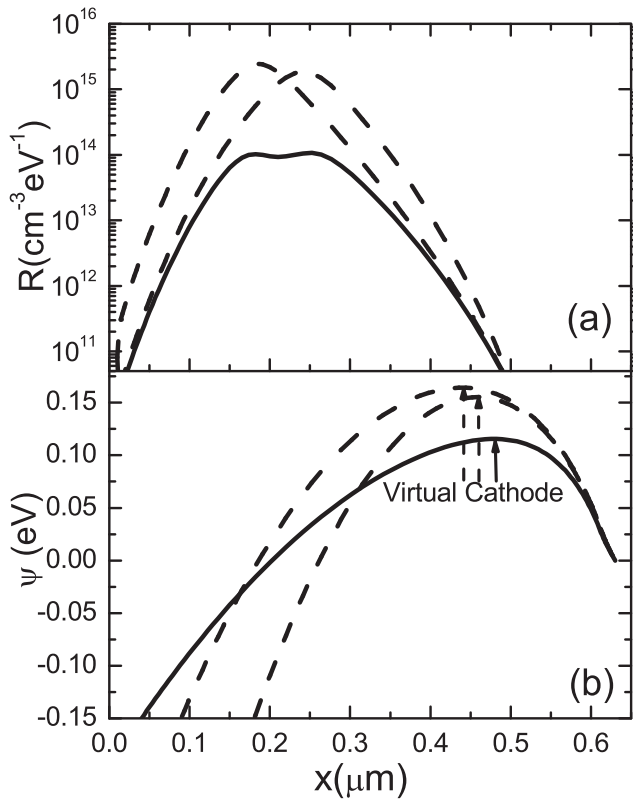

FIG. 6. Changes in (a) the recombination rate at a forward voltage of 0.1 V (b) and in the electron potential profile at a forward voltage of 2 V both under dark conditions when the Meyer-Neldel energy is assumed 150 meV at the neutral donor-like and acceptor-like defect states (dashed lines). The recombination rate and potential profiles where the MNB is not taken into account are shown for comparison (solid lines).

Under illuminated conditions, the increase of either capture cross section for electrons or holes at neutral acceptor or donor defect states, respectively, by the MNB significantly magnifies the recombination losses that severely deteriorate J_{SC}, FF, and V_{OC} as it can be observed in Figure 5(b) for Meyer-Neldel energies of 150 meV. The increase of the recombination rates is illustrated in Figure 3(c) at short circuit conditions under AM1.5 illumination. It is interesting to note that: (a) the maximum increase of the recombination rate takes place in the front region of the intrinsic layer when the MNB is taken into account at neutral acceptor-like defect states and in the back region of the intrinsic layer when the MNB is taken into account at neutral donor-like defect states and (b) the recombination rate increases more when the MNB is implemented in neutral donor-like defect states than in neutral acceptor-like defect states. These are the regions where the products $\sigma_n^0 n$ and $\sigma_p^0 p$ show their minimums before the MNB is implemented. Furthermore, charged capture cross sections are higher than neutral capture cross sections, i.e., $\sigma_p^- > \sigma_n^0$ and $\sigma_n^+ > \sigma_p^0$ before the MNB is implemented. Electrons are minority carriers at the front region of the intrinsic layer and holes at the back region of the intrinsic layer. As the intrinsic layer is really slightly n-type, the Fermi level is closer to the conduction band edge than to the valence band edge under equilibrium conditions. In order to

have a n-type material, Gaussian distributions should be placed asymmetrically with respect to the band edges: the ones with acceptor-like states should be situated closer to the conduction band edge than the ones with donor-like states with respect to the valence band edge. Hence, capture cross sections of neutral donor-like defect states will increase more than capture cross sections of neutral acceptor-like defect states when the MNB is implemented because donor-like traps are comparatively deeper in energy. In a previous contribution about the electron drift mobility, the impact of the MNE in defect states was minimized by adopting very high Meyer-Neldel energies of 1000 meV.[17]

In optical detectors, the MNB implemented in either donor-like or acceptor-like defect states gives rise to a significant increase of the reverse dark current due to the enhancement of the thermal generation of e-h pairs, while under illumination there is an important drop of the collected current due to the increase in the recombination losses taking place especially at low forward voltages.

Being more specific when the MNB is included in capture cross sections of either donor-like or acceptor-like defect states, very high values for the MNEs not below 2000 meV have to be adopted in order to keep the relative differences below 15% in dark J-V curves and below 4% in light J-V curves. MNEs of 1000 meV increase these differences to nearly 28% in the high forward dark J-V and 8% in the light J-V.

The transit currents associated by emission and trapping of electrons (holes) between donor (acceptor)-like defect and extended states cannot be detected in the time scale used in TOF experiments. However, in solar cells and optical detectors operating under steady state conditions no restrictions apply to the times associated to these transitions. There is no logical reason to restrain the MNB to only two of the four possible emission processes (Eq. (8)). If charged capture cross sections are also affected by the MNB, the modifications of the dark and light J-V become extreme (Eqs. 8(a) and 8(d)). The impact of including the MNB in capture cross sections of both neutral and charged states is illustrated in Figure 7 for the light J-V under AM1.5 irradiation.

The departure from the experimental light J-V becomes even more severe when the MNB is included at charged capture cross sections of tail states rather than at defect states because tail states are further in energy than defect states from the opposite band edges. Hence, our results indicated that the MNB is completely inapplicable in solar cell and optical detector modeling when both neutral and charged capture cross sections are assumed to follow the energy dependence proposed in the MNB. The predicted solar cell efficiencies become extremely poor. Severe drops can be observed in the three parameters J_{SC}, FF, and V_{OC}. Excessive dark currents and poorly collected photocurrents are also predicted in optical detectors that become far away from the expected figures.

VI. MEYER-NELDEL BEHAVIOR OF EMISSION COEFFICIENTS AT TAIL STATES

Trapping and recombination are more significant at the valence band tail than at the conduction band tail due to its wider slope and to the lower hole mobility. Our previous results demonstrate that fittings of J-V curves cannot be preserved when the MNB is implemented in deep states because of the exponential dependence of capture cross sections with energy depth. On the other hand, shallow states like acceptor-states of the conduction band tail could show the MNB without impacting on device performance. Hence, there should be an energy that separates states showing and not showing the MNB. Our fittings of experimental J-V curves can be maintained only when tail states of the valence band, shallower in energy than $E_{DT\text{-}MNB}$ ~0.37 eV–0.39 eV are assumed to show a MNB. When the MNB is implemented in neutral capture cross sections of deeper donor-like states our fitting of the J-V curves cannot be recovered by changing our input parameters. The values of $E_{DT\text{-}MNB}$ correspond to a lowering of the solar cell efficiency in 1% and 2%, respectively, being the standard of 1% safer than 2%. In TOF measurements, the state of quasi-equilibrium with extended states is achieved only by localized states with energies E_T such as $E_V < E_T < E_{DED\text{-}V}$, where $E_{DED\text{-}V}$ is the demarcation energy $E_{DED\text{-}V}$ (Eqs. 4(b) and 9). The TOF technique cannot test whether the emission coefficients of traps deeper than $E_{DED\text{-}V}$ show a MNB or not. Chen *et al.*[8] presented Monte Carlo simulations of multiple-trapping with the MNB in a-Si:H assuming an exponential band tail and found the best fit for $E_{MND\text{-}V} = 70$ meV and $\omega_{00D} = 6.5 \times 10^{10}$ s^{-1}.[8] Using Eq. (9), a demarcation energy of $E_{DED-V} \sim 0.426$ eV is obtained for $t_H = 5 \times 10^{-7}$ s. The transit time was evaluated as in the paper of Tiedje and Rose (Eq. (10) of Ref. 16) and it is within the experimental values published by Marshall (at 295 K) in his TOF measurements.[27] The density of states at energies $E_V < E_T < E_{DED-V}$ is controlled by tail states (see Figure 2). However, holes trapped at the particular energy $E_{DED\text{-}V}$ will only have at most, one chance of being trapped and reemitted within the transit time t_H. In order that localized states could achieve a real state of quasi-equilibrium with extended states, free holes should have the chance of being trapped and released several times before exiting the p-i-n device. This scenario can be created by

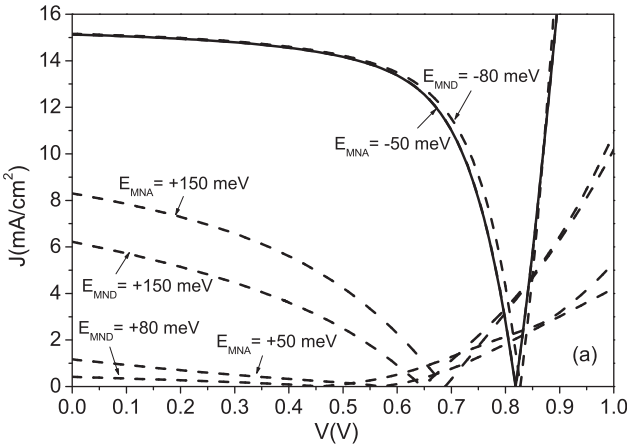

FIG. 7. Light J-V characteristics when the MNB is taken into account in capture cross sections not only of neutral but also of charged tail states and defect states (dashed lines) for Meyer-Neldel energies of 50 meV and 80 meV at acceptor-like and donor-like tail states, respectively, and 150 meV at defect states. The light J-V characteristic when the MNB is taken into account is shown as a solid line for comparison.

replacing the time t_H of Eq. (10) for a shorter time. The energies $E_{DT\text{-}MNB}$ and $E_{DED\text{-}V}$ can be made to coincide replacing t_H in Eq. (10) by one third of t_H. In TOF experiments, the MNB of deeper states cannot be explored. Hence, our assumption of deeper states not showing a MNB is not conflicting with findings made with the TOF technique. Using a similar reasoning for neutral capture cross sections of acceptor-like states, the corresponding energy $E_{AT\text{-}MNB}$ was evaluated as $E_{AT\text{-}MNB} \sim 0.456$–$0.484$ eV due to the lower slope of the conduction band tail and the higher free electron mobility. The demarcation energy $E_{DEA\text{-}C}$ at the conduction band tail can be estimated as $E_{DEA\text{-}C} \sim 0.4$ eV ($E_{MNA\text{-}C} = 40$ meV,[8] $\omega_{00A} \sim 5 \times 10^9$ s^{-1},[8] and $t_H = 5 \times 10^{-8}$ s, Refs. 16 and 28). The density of states at energies $E_{DEA\text{-}C} < E_T < E_C$ is mostly controlled by tail states (see Figure 2). Hence, for acceptor-like states there is no conflict between the results obtained with TOF and our assumption of deeper states with no MNB.

The difficulties introduced by the implementation of the MNB in device modeling motivated in us to explore the anti MNB where the Meyer-Neldel energy is assumed to be negative.[7] There are few contributions where the anti MNB was reported in disordered semiconductor films and devices.[22–26] In Sec. VII, results of the effect of the anti MNB in device modeling are shown and briefly discussed.

VII. ANTI MEYER-NELDEL BEHAVIOR IN EMISSION PRE-FACTORS OF TAIL STATES

Negative Meyer-Neldel energies are associated to lower cross sections at deeper gap states. Hence, the opposite trend should be predicted, i.e., better device performances.

First, the scenario where only neutral capture cross sections are changed was explored. As for positive MNEs when the anti MNB is applied only to neutral capture cross sections of acceptor tail states, there is no any visible impact in the dark and light J-V characteristics. When neutral capture cross sections for holes at donor tail states are assumed lower at deeper energies the dark J-V is not affected, while the light J-V shows a better FF and a little higher V_{OC} due to the decrease of the recombination rate through neutral donor states (see Figure 3(b)). In Figures 4(a) and 5(a), the dark and light J-V predicted by D-AMPS are shown when the anti MNB is implemented for a MN energy of -30 meV (to make more visible the effect) and -70 meV respectively. In the SRH formalism, the probability of emission of holes from donor-like tail states to the conduction band is much lower than the probability of emission of holes to the valence band, due to the exponential dependence with respect to the trap energy (Eq. (3)). A similar statement can be made when the probability of emission of electrons from acceptor-like tail states to the valence and to the conduction band is compared. The anti MNB increases the asymmetry between these two probabilities because charged cross sections of deeper states will be set up to even lower values by the anti MNB. Hence, the anti MNB does not significantly alter the predicted J-V characteristics when both neutral and charged capture cross sections are modified accordingly.

The inclusion of the anti-MNB can facilitate the matching of FF in light J-V characteristics of a-Si:H solar cells with thick intrinsic layers especially when the Defect Pool is invoked to model the density of DBs. In a previous contribution, the light J-V of a a-Si:H p-i-n cell with a 600 nm thick intrinsic layer was matched by adopting an optimistic hole mobility μ_P of 4 cm^2 V^{-2} s^{-1}.[11] When the hole mobility is lowered to $\mu_P = 2$ cm^2 V^{-2} s^{-1}, a more widely accepted value, FF drops significantly, while Voc and Jsc change to less extent. The inclusion of the anti-MNB for $\mu_P = 2$ cm^2 V^{-2} s^{-1} gives rise to a light J-V similar to the one obtained with $\mu_P = 4$ cm^2 V^{-2} s^{-1} without MNB (see Figures 5 and 8).

It is interesting to remark that our solar cell simulations show a more linear relationship J_{SC}-V_{OC} in a-Si:H p-i-n solar cells[29] and in the dependence of J_{SC} with the light source intensity, that becomes more notorious below room temperature, when the anti-MNB rather than the MNB is implemented in donor-like tail states.

VIII. FINAL COMMENTS

This impact of the MNB was also analyzed in a-Si:H based p-i-n devices with other intrinsic layer thicknesses and with a buffer layer at the p/i interface deposited and characterized also at Delft University. Structures with 200 nm, 400 nm, and 600 nm thick intrinsic layers were fitted with the SRH formalism, modeling the density of defects with either the UDM or the DPM.[11,30] Trends obtained when the MNB and anti-MNB were taken into account in the different neutral capture cross sections were entirely similar to the ones already discussed. Deviations of the J-V curves predicted with the MNB are smaller in devices with thinner intrinsic

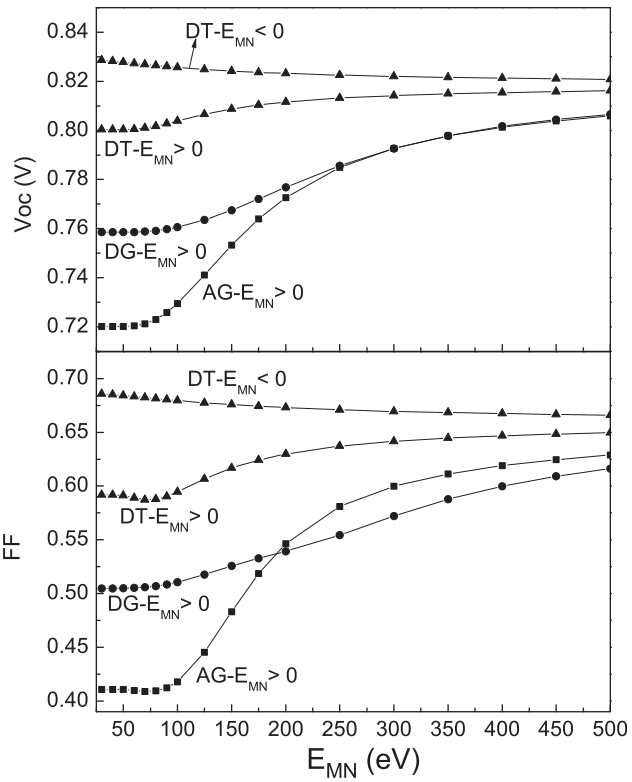

FIG. 8. Predicted V_{OC} and FF with respect to the Meyer-Neldel energy adopted in neutral donor tail states (DT-triangles), acceptor defect states (AG-squares), and donor defect states (DG-circles) when the physics of the MNB is included in our formalism.

layers due to the stronger electric field that makes J-V curves less sensitive to traps. When the DPM is invoked, the departures are more pronounced than when the MNB is implemented in neutral capture cross sections of defect states because a higher density of DBs is generated inside the intrinsic layer. Similar results were also obtained when the MNB was implemented in charged capture cross sections.

IX. CONCLUSIONS

The impact of including the MNB in the emission probabilities of free carriers from gap states to extended states in the output characteristic curves of solar cells and optical detectors was explored with computer device modeling. The MNB can be realized by adopting energy dependent capture cross sections that exponentially increase with the gap state energy depth with the slope given by the Meyer-Neldel energy. The MNB does not impact in the calculation of the J-V characteristics of p-i-n a-Si:H based devices when all neutral capture cross sections for electrons at acceptor-like tail states are assumed to be energy dependent. On the other hand, the MNB leads to the prediction of poor solar cell and detector performances, well below the experimental figures, when all neutral capture cross sections for holes at donor-like tail states and especially when all neutral capture cross sections at defect states are assumed to be energy dependent. The predicted performances become extremely low and unrealistic when the MNB is included in both neutral and charged capture cross sections of gap states. Hence, device modeling of thin film solar cells and optical detectors shows that the emission coefficients of all gap states cannot simultaneously show a MNB. The physics of the MNB can only be taken into account at shallow states not further from 0.45 eV and 0.37 eV from the conduction and valence band edges, respectively, that can be associated with the scenario of quasi-equilibrium described in TOF measurements. The normal MNB cannot be implemented in deeper states except by adopting very large Meyer-Neldel energies ($\sim$1000 meV), a similar scenario to assume no MNB at all. The implementation of the anti MNB, consisting in assuming negative Meyer-Neldel energies at tail states, leads to prediction of slightly better and reasonable performances in solar cells and optical detectors. The anti-MNB in solar cells increases FF and to a lesser extent Voc and J_{SC}, as observed in our simulations when the hole extended state mobility is increased.

ACKNOWLEDGMENTS

We highly appreciate the financial support of CONICET and Agencia Nacional de Promoción Científica y Tecnológica through the grants and PIP-112-201101-01052 and PICT-2013 2098 respectively. I would also like to thank members of the Department of Photovoltaic Materials and Devices of Delft University of Technology, the Netherlands, for providing the experimental information, C. Longeaud, from Laboratoire de Génie Electrique de Paris, for helpful discussions, and Marcelo de Greef for reorganizing our figures.

[1]V. Halpern, Philos. Mag. B **54**, 473 (1986).
[2]V. Suntharalingam and H. M. Branz, in *Amorphous Silicon Technology* (Mater. Res. Soc. Symp. Proc., 1994), Vol. 336, p. 153.
[3]E. Klimovsky, J. K. Rath, R. E. I. Schropp, and F. A. Rubinelli, Thin Solid Films **422**(1–2), 211 (2002).
[4]J. A. Willemen, "Modelling of amorphous silicon single- and multi-junction solar cells," Ph.D. thesis (Delft University of Technology, 1998).
[5]A. Yelon, B. Movaghar, and R. S. Crandall, Rep. Prog. Phys. **69**, 1145 (2006).
[6]H. Antoniadis and E. A. Schiff, Phys. Rev. B **46**, 9482 (1992).
[7]T. Kagawa and N. Matsumoto, Philos. Mag. B **51**, 273 (1985).
[8]W.-C. Chen, L.-A. Hamel, and A. Yelon, J. Non-Cryst. Solids **220**, 254 (1997).
[9]R. S. Crandall, Phys. Rev. B **43**, 4057 (1991).
[10]E. A. Schifff, Philos. Mag. B **89**(28–30), 2505 (2009).
[11]M. de Greef and F. Rubinelli, Phys. Status Solidi B **252**, 170 (2015).
[12]T. Tiedje, Semicond. Semimet. **21**, 207 (1984).
[13]R. N. Hall, Phys. Rev. **83**, 228 (1951).
[14]W. Shockley and W. T. Read, Phys. Rev. **87**(5), 835 (1952).
[15]R. A. Street, *Hydrogenated Amorphous Silicon* (Cambridge University Press, 1991).
[16]T. Tiedje and A. Rose, Solid State Commun. **37**, 49 (1981).
[17]H. Ramirez and F. Rubinelli, "Electron drift mobility of hydrogenated amorphous silicon evaluated with device computer modeling at steady state conditions," Thin Solid Films (submitted).
[18]F. Rubinelli, J. Rath, and R. Schropp, J. Appl. Phys. **89**, 4010 (2001).
[19]R. Kind, R. A. C. M. M. van Swaaij, F. Rubinelli, S. Solntsev, and M. Zeman, J. Appl. Phys. **110**, 104512 (2011).
[20]M. Powell and S. Deane, Phys. Rev. B **53**, 10121 (1996).
[21]R. A. Street, Appl. Phys. Lett. **41**(11), 1060 (1982).
[22]S. K. Ram, S. Kumar, and P. Roca i Cabarrocas, J. Non-Cryst. Solids **354**, 2263 (2008).
[23]H. Meiling and R. E. I. Schropp, Appl. Phys. Lett. **74**, 1012 (1999).
[24]R. Flückiger, J. Meir, M. Goetz, and A. Shah, J. Appl. Phys. **77**, 712 (1995).
[25]H. Overhof and W. Beyer, Philos. Mag. B **47**, 377 (1983).
[26]R. Widenhorn, A. Rest, and E. Bodegom, J. Appl. Phys. **91**, 6524 (2002).
[27]J. M. Marshall, R. A. Street, J. Thompson, and W. B. Jackson, Philos. Mag. B **57**(3), 387 (1988).
[28]J. M. Marshall, R. A. Street, and J. Thompson, Philos. Mag. B **54**(1), 51 (1986).
[29]J. M. Pearce, R. J. Koval, R. W. Collins, and C. R. Wronski, in *Proceedings of the 28th IEEE Photovoltaic Specialists Conference, Alaska* (2000), p. 988.
[30]M. de Greef, F. Rubinelli, and R. A. C. M. M. van Swaaij, Thin Solid Films **540**, 227 (2013).